Examination of the LPBF Process by Means of Thermal Imaging for the Development of a Geometric-specific Process Control

T. Pichler*, J.H. Schleifenbaum*†
*Fraunhofer Institute for Laser Technology ILT, Aachen (Germany)
† Chair for Digital Additive Production DAP at RWTH Aachen University (Germany)

Abstract

The development of process parameters for the Laser Powder Bed Fusion (LPBF) process is typically carried out by the manufacturing and metallurgical analysis of geometrically primitive test specimens (e.g. cubes). The process parameters identified in this way are used for the manufacturing of parts which are characterized by a high geometric complexity and a combination of solid and filigree component areas. Due to the discrepancy between the parameter development on primitive specimens and applications with complex parts, a geometric-specific process control is to be developed. In the context of this work different sample geometries are manufactured from Ti6Al4V by LPBF and the process is monitored by thermal imaging. The influence between component geometry and process parameters on the thermal behavior is shown.

Introduction

In the Laser Powder Bed Fusion (LPBF) process, parts are additively manufactured from metal powder. Powder layers with a thickness of typically 20 μm to 100 μm are selectively melted using laser radiation and locally solidified. The repetitive process of powder application and selective melting produces parts in layers. Due to the additive manufacturing principle, components of almost unlimited complexity can be manufactured. LPBF is used in numerous industries such as the automotive industry, aerospace, medical technology and turbo machinery. [1]

The deficiencies of the LPBF process include the build time, which sometimes takes several days to complete, and the relatively low process robustness. [2, 3] In addition to an adaptation of the machine technology, there is the research question of whether these aspects can also be addressed by a further development of the actual LPBF process. One possible approach is to adapt the LPBF process control to the part geometry.

In the following, an approach for adapting the LPBF process control to the pat geometry using the material Ti-6-Al4-V as an example is discussed. Experiments on the influence of geometry in the area of a layer of the component (2D-Area) and in the area of already built component areas (3D-Area) are presented as examples. The investigations are carried out using a thermographic camera to display the temperature field within the LPBF process zone.

State of the Art

Approaches for the adaptation of the process control to the component geometry were examined e.g. by means of the High Power SLM. The component is divided into a skin and a core area. The core area is processed with a higher layer thickness (typically 2-3 times higher) as well as a laser beam with TopHat intensity profile and a diameter of 500 μm to 1000 μm at laser powers in the kW range in order to achieve the highest possible build-up rate. In order to maintain the

highest possible surface quality, the skin area is processed with a single-mode fiber laser with a maximum nominal power output of 400 W and a laser beam diameter of approx. 90 μm. [2]

The system manufacturer EOS GmbH enables users of its EOSPrint 2.0 software to adjust the laser power as a function of the scan vector length using a scaling factor. [4]With this approach, overheating can be avoided, e.g. by reducing the laser power of short vectors in narrow areas of the part.

Using the Advanced ToolPath Utility of the AutoDesk Netfabb software, a JavaScript programming interface can be used to individually control path creation. Depending on the machine type, the process parameters can also be adjusted [5]. Compared to the current state of the art, the software enables an extended adaptation of the process parameters and the build strategies, so that different areas of the part can be processed with adapted process strategies.

In [6] a thermographic camera is used to monitor the LPBF process in order to automatically detect spatter particles in the process zone. In addition, the effect of a variation of the process parameters laser power, scanning speed and hatch distance on the emission detected by the thermographic camera is displayed. The change in the length of the scan vectors induced by the scan strategy and the resulting temperature field with overheating effects when the scan vector length is shortened are also shown as examples.

In [7], a thermographic camera under the processing of the material IN718 is used to determine the dimensions of the melt pool as a function of the scanning speed. A reduction of the melt pool width with an increase of the scanning speed is observed. A correlation between scanning speed and length of the melt pool cannot be proven.

Approach

Geometric-specific Process Control

A prerequisite for the development of a geometric-specific process control for the LPBF process is its applicability to any components and geometry types. The approach presented here is to adapt the LPBF parameters on two levels: On the one hand by analyzing the currently exposed layer, the so-called 2D-Area, and on the other hand by analyzing the already built component areas, the so-called 3D-Area. LPBF process parameters are then developed for both areas by manufacturing and analysing specific test specimens.
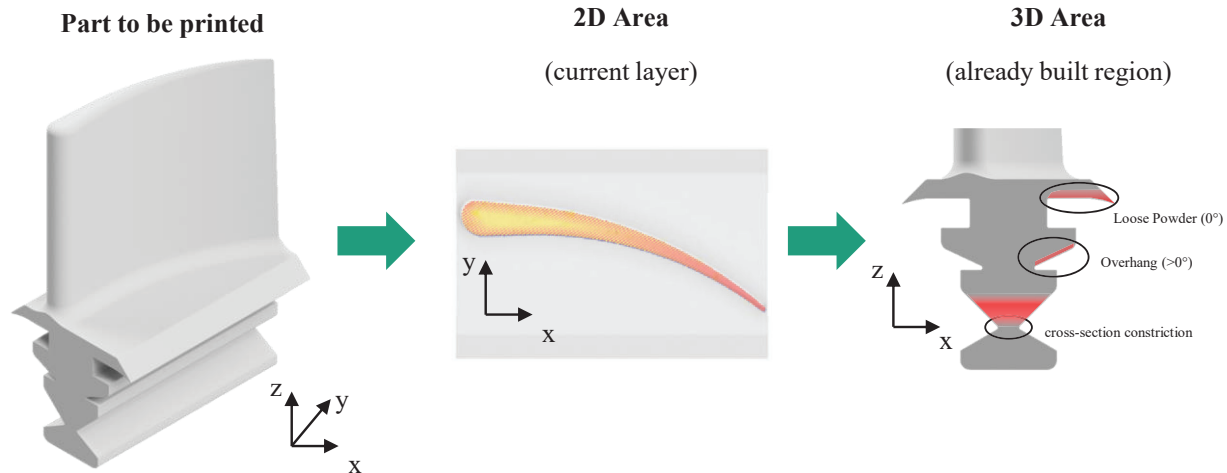
Part to be printed

2D Area
(current layer)

3D Area
(already built region)

Loose Powder (0°)

Overhang (>0°)

cross-section constriction

Figure 1: Approach of the geometric-specific process control

2D-Area

The exposure of a layer within LPBF is characterized by vector paths that are traced with a typically focused laser beam at a given power and speed. Depending on the geometry of the component, this results in a profile of temporal and spacial energy input. For the description of this temporal and spacial energy input, the repetition time can be used as a key figure: It describes the time that elapses until a point within the layer is reheated by its adjacent melt track. Figure 2 shows false color images of one layer in different components.
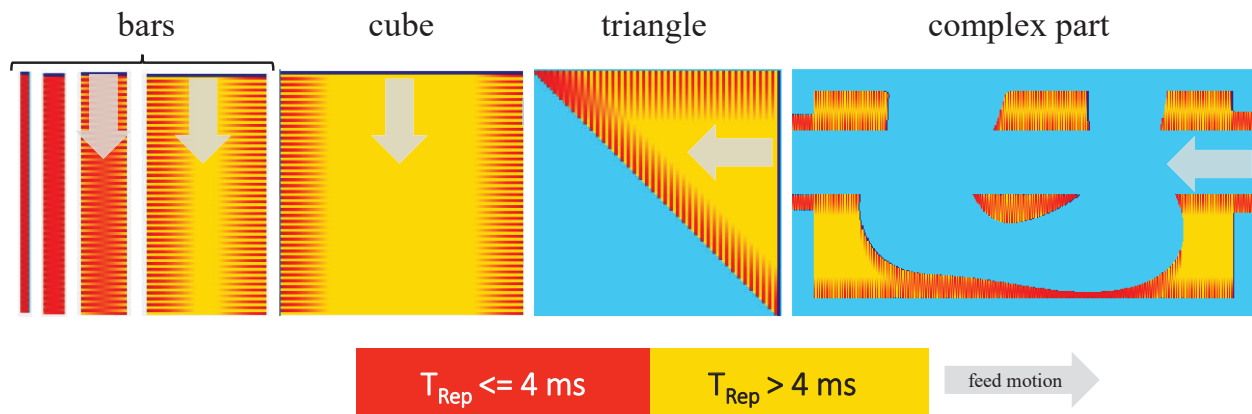

bars   cube   triangle   complex part

T_{Rep} <= 4 ms T_{Rep} > 4 ms   feed motion

Figure 2: Repetition times of different components in false colors representation

The current layer is processed meanderingly by the laser beam in the direction of the indicated feed motion. Areas with a repetition time less than or equal to four milliseconds are marked red, areas with a repetition time greater than four milliseconds are marked yellow. The repetition time is used to identify those areas within a layer where overheating is likely and adjustment of process parameters could be beneficial. In this example, the repetition time was initially chosen arbitrarily to explain how the model works. On an experimental level, the critical repetition time must be determined.

3D-Area

For the investigation of already built component areas, the component can first be divided into a so-called voxel (volumetric pixel) model, as shown in Figure 3.
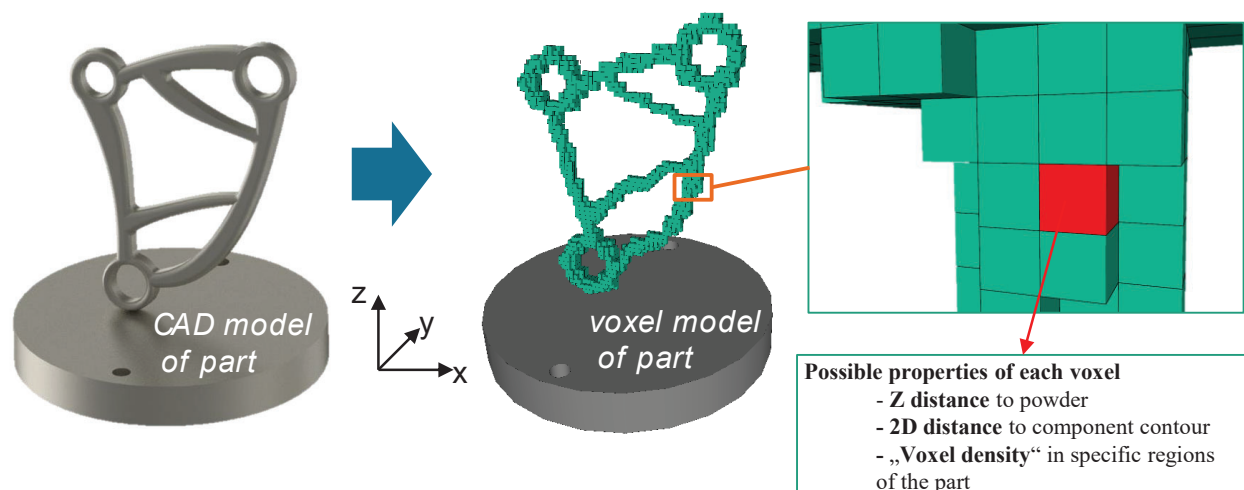
Figure 3: CAD and corresponding voxel model of a part to be manufactured by LPBF

Properties can then be assigned to each voxel to characterize the geometric properties of the part at the corresponding location. Possible properties of a voxel can be e.g. the distance to the powder in Z-direction, the 2D- and 3D-distance to the component contour or the voxel density as a measure for the filigree of the component. The LPBF process parameters can then be adjusted depending on the voxel properties. For example, for filigree areas with a relatively low voxel density, the energy input can be reduced by decreasing the laser power or increasing the scanning speed in order to avoid overheating.

Methodology

In the following, various samples for the 2D range and the 3D range will be manufactured and the process emissions recorded with a thermal imaging camera.

Experimental Setup

The experiments will be performed on an LPBF laboratory machine. Figure 4 shows the technical specifications and a picture of the system.
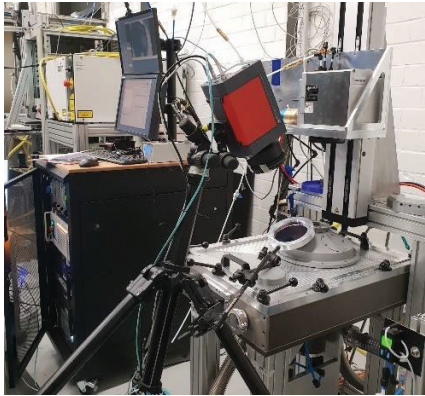
Build Area	Build platform diameter: 98 mm Build height: 150 mm		Powder Material	Ti6Al4V
Laser	Singlemode Fibre Laser Max. Power: 400 W (cw) Wavelength: 1080 nm		Particle Size distribution	15 μm – 45 μm
Optical System	Scanlab HurryScan20, Scanlab VarioScan40 Spot Size: 75 μm		Powder Supplier	PraxAir Surface Technologies
Shielding gas	Argon < 50 ppm O_2 during process		Laser Power* Scan Velocity* Hatch Distance*	265 W 1200 mm/s 0.12 mm
Powder deposition	Bottom-Loader, soft-recoater (silicone)		Scanning Strategy*	Meander, 90° increment, feed direction always against inert gas flow
Modification	chamber cover with viewing window for thermographic camera (ZnSe Window)		*Standard Parameters from preliminary experiments to achieve a porosity of less than 0.5 %	

Figure 4: Technical data and illustration of the LPBF laboratory machine, material data and standard process parameters

2D-Area

For the 2D-Area 10 mm long webs of different widths (10 mm, 5 mm, 2.5 mm, 1 mm, 0.5 mm) are manufactured (Figure 5).
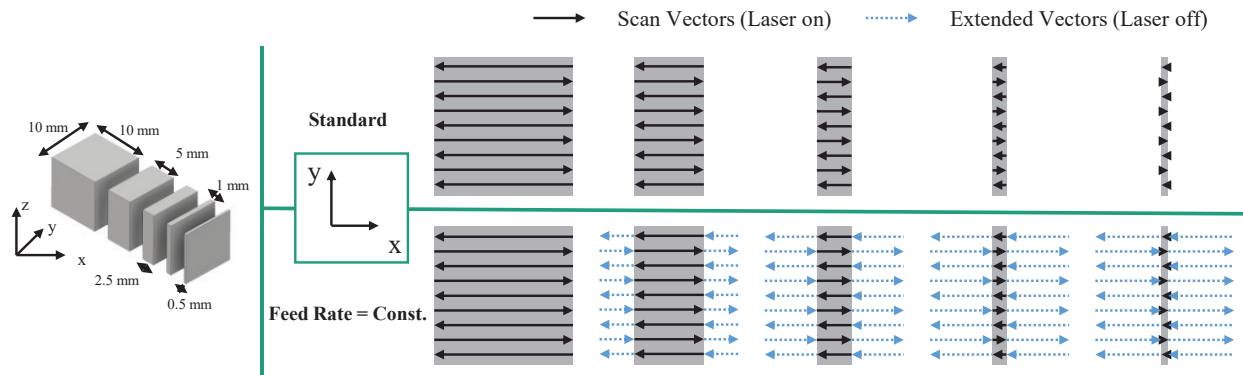

Figure 5: Schematic depiction of webs of different widths with variable and constant feed speed

The webs are manufactured with standard parameters on the one hand and with a constant feed rate on the other hand. The constant feed rate corresponds to the feed rate for the web with the dimensions 10 mm X 10 mm. In order to implement the constant feed rate, the vectors of the shorter webs are extended, but the laser is switched off earlier, so that the desired web width is achieved. The extended vectors are dashed in Figure 5. The evaluation is carried out by qualitative examination and comparison of the false color representation of the thermographic image data.

3D-Area

To examine the 3D-Area, cube-shaped test bodies are placed on beams and the side length of the individual beams is varied to achieve different surface transition ratios (TR). Figure 6 schematically shows the specimens produced and the surface transition ratios set in each case.
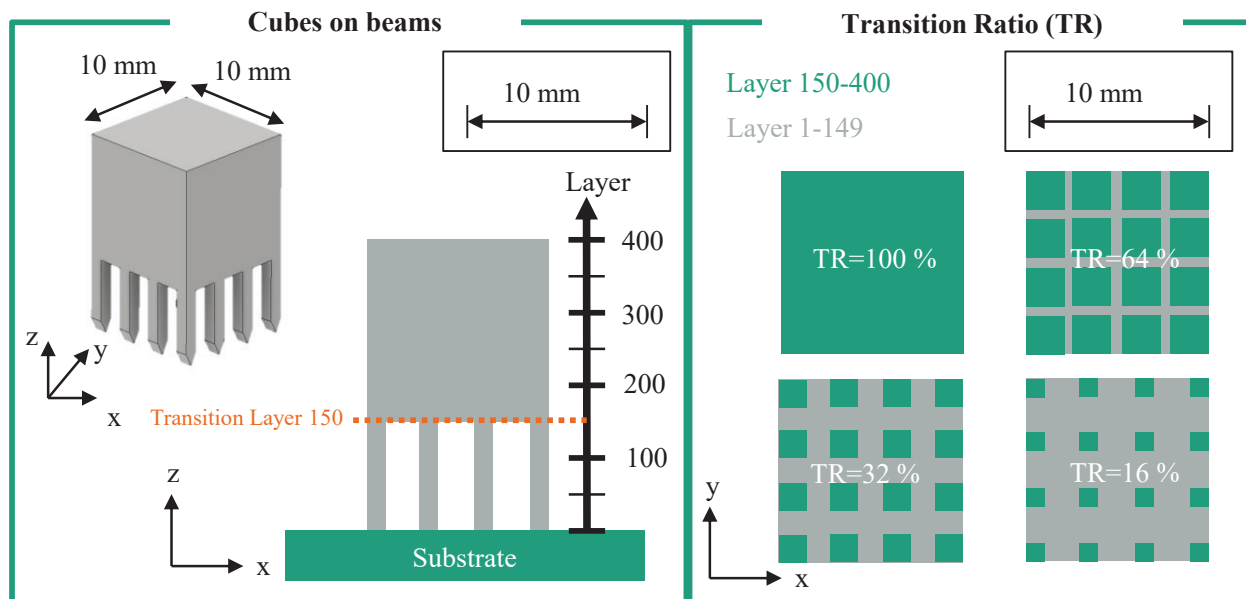

Figure 6: Test specimen for examination of the 3D-Area

The specimens are manufactured with standard parameters on the one hand and with variation of the laser power (250 W, 200 W, 150 W, 100 W) on the other hand. For evaluation, a 10 mm X 10 mm measuring field is placed in the exposed area of the specimen and its mean emission value over time is calculated.

Results

2D-Area

Figure 7 shows the thermographic images of the exposure within a layer of the web structures of different widths.
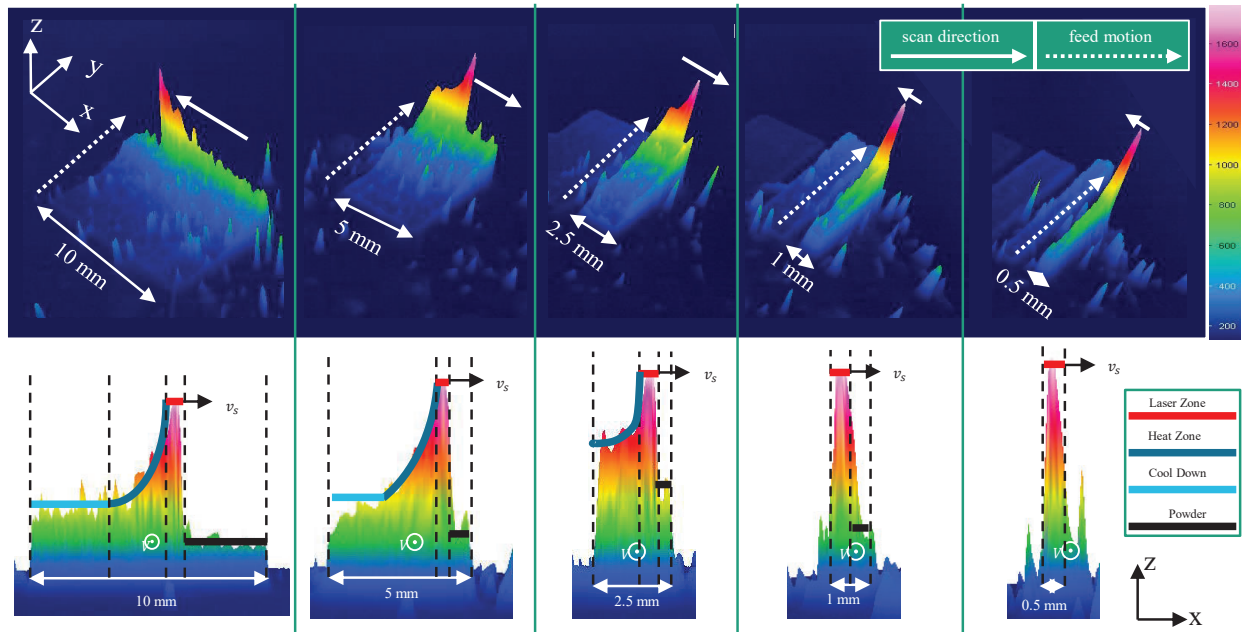

Figure 7: Thermographic images of the exposure within a layer of web structures of different widths

In the upper part of figure 7 a perspective view of the exposure of the web structures is shown. In the lower part a side view of the melt front of the web structures is shown, with the feed direction pointed into the image plane. On the basis of the web with a width of 10 mm, the melt front can be divided into 4 temperature zones: The laser zone, a subsequent heat zone and a subsequent cool down zone. Seen in the scanning direction in front of the laser-affected zone, the area of the powder that has not yet melted is also located.

With the reduction of the web width, the characteristics of the melt front and the temperature zones change: First, the cooling zone becomes shorter until it is virtually non-existent at a web width of 2.5 mm. With this web width, only the laser influence zone, heat zone and powder zone are present. If the web width is further reduced to 1 mm and 0.5 mm respectively, the heat zone also disappears. Only the laser-affected zone and a very small area of the powder zone remain.

With the reduction of the web width, in addition to the above described change in the characteristic of the melt front in the scanning direction or X-direction, a change in the characteristic in the feed direction or Y-direction also occurs. Figure 7 already shows that the edge

steepness of the temperature field flattens in the Y-direction with a reduced web width. Figure 8 shows the thermographic images of the web structures in top view.
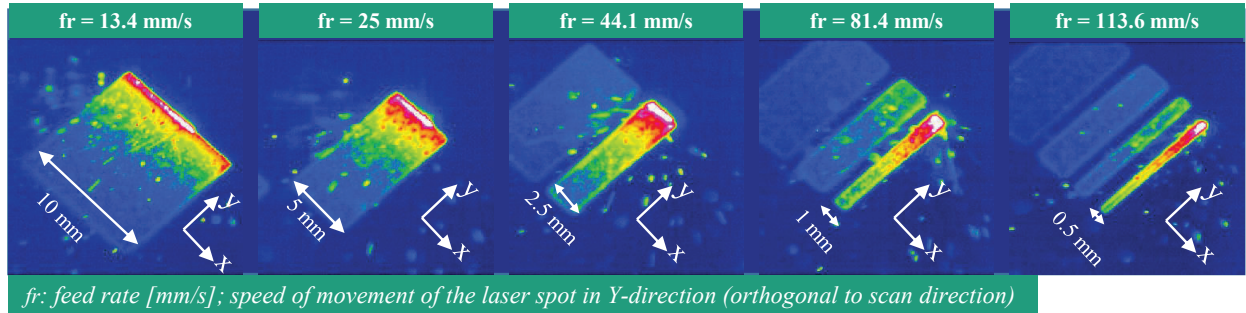

fr: feed rate [mm/s]; speed of movement of the laser spot in Y-direction (orthogonal to scan direction)

Figure 8: Thermographic images of web structures in false color representation manufactured with standard parameters

With the reduction of the web width, the heat-affected zone is shifted further in the Y-direction: Whereas the heat-affected zone of the 10 mm wide web extends approx. 2.5 mm – 3 mm in the feed direction, the heat-affected zone of the relatively narrow 1 mm or 0.5 mm wide webs extends over the entire 10 mm Y-dimension of the web. The global movement direction of the laser spot shifts from the X-direction to the Y-direction with decreasing web width, as the increasing feed rate illustrates. The web with a width of 0.5 mm appears to have a similar characteristic to a single track, but with movement in the Y-direction. However, a comparison of the resulting line generation reveals significant differences: A single track with standard parameters results in a line energy of

$$E_{Track,X} = \frac{250\,W}{1200\,\frac{mm}{s}} = 0.21\,\frac{J}{mm}.$$

The comparable line energy in Y-direction for a web with 0.5 mm width and a feed rate of 113.6 mm/s results in

$$E_{Track,Y} = \frac{250\,W}{113.6\,\frac{mm}{s}} = 2.2\,\frac{J}{mm}.$$

The line energy of the 0.5 mm web in the Y-direction is greater by a factor of 10 than the energy per unit length in the X-direction. The energy per unit length of the 0.5 mm web in the Y-direction is greater by a factor of 10 than the energy per unit length in the X-direction. This can be a possible explanation for the changed thermal profile as well as a potential source of overheating with correspondingly filigree structures.

Figure 9 shows thermographic images of web structures, in the upper image area with standard parameters, in the lower image area with constant feed rate. Areas with an emission value greater than 600 are colored red, areas with a lower emission value are colored grey.
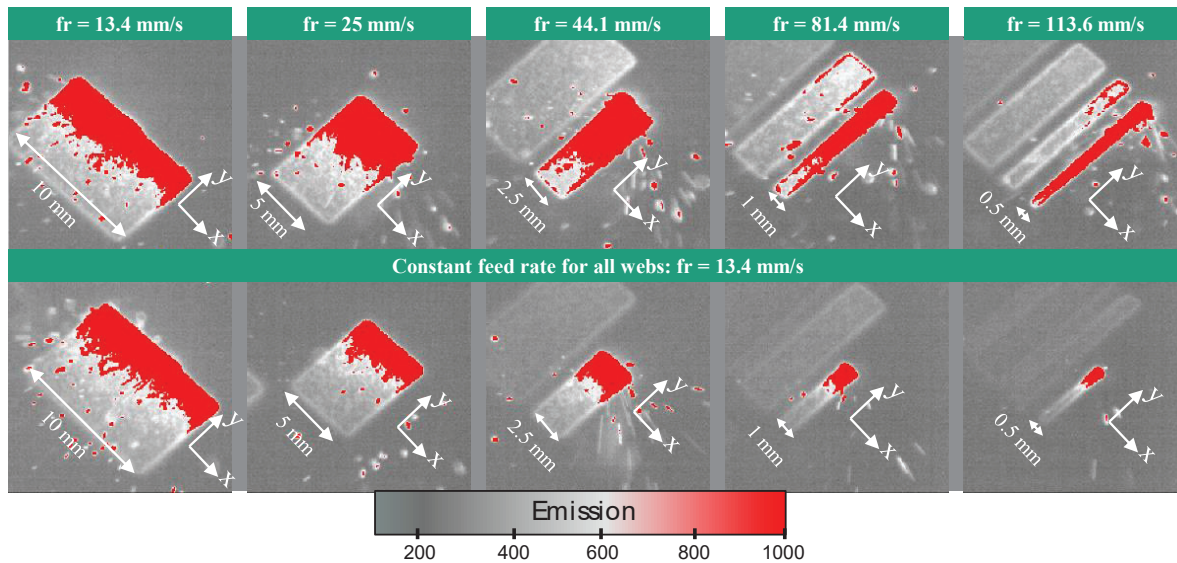
Figure 9: Thermographic images of web structures, upper image area: standard parameters, lower image area: constant feed rate.

In the upper row of Figure 9, the displacement of the heat-affected zone in the Y-direction with decreasing web width already visible in Figure 7 can be seen. In the lower row, the heat-affected zone is equalized by extending the scan vectors. The expansion of the heat-affected zone in the Y-direction can be completely adjusted and is independent of the web width.

3D-Area

Figure 10 shows the average emission values for the transition layer between the beam area and the massive area of the specimen (layer 150) for different area transition ratios over time.
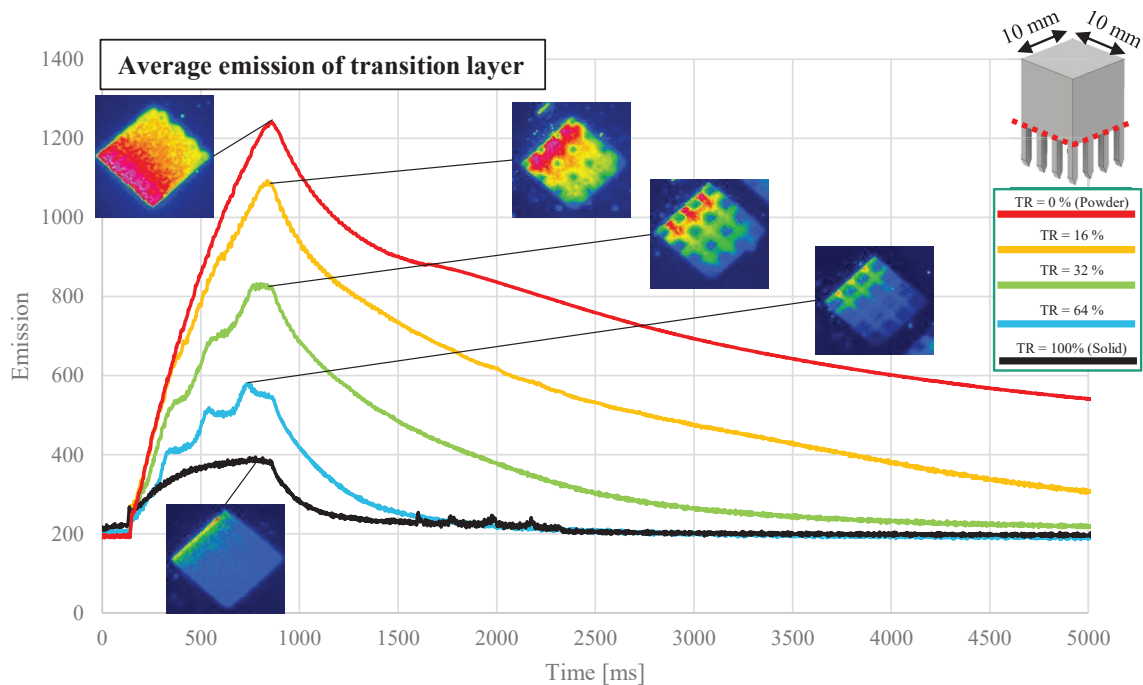

Figure 10: Average emission of transition layer for different transition ratios

In addition to the cubes on beams, the courses of the emission values for the exposure of a solid cube and loose powder are also shown. All specimens rise to a peak value during the exposure in a timeframe of up to t = 860 ms, after which the cooling begins. When comparing the two extreme cases, the peak emission value lies between 1240 (loose powder) and 390 (solid cube), and are thus more than a factor of 3 apart. The emission values of the cubes on bars lay in between of these extreme values, whereby the peak temperature drops with increasing surface transition ratio. As the surface transition ratio decreases, heating rate of the specimens increases during exposure. Especially for the cubes specimens with TR = 64 % and TR = 32 %, a kind of staircase effect is visible during exposure or heating. This results from the alternating exposure of areas with beams and areas with loose powder. It becomes clear that the heat dissipation in solid areas such as in the area of the beams or the solid cube is significantly greater than in areas with loose powder.

Figure 11 shows the peak values of the mean emission over several layers, starting from the transition layer (layer 150) for the cubes on beams with different area transition ratios and for the solid cube as reference body. For metrological reasons, it was not possible to perform a measurement for each individual layer, so that the measurement points are separated by several layers. For all surface transition ratios it becomes clear that the relatively large overheating effects observed in the transition layer (layer 150) have already largely subsided after approx. 20 layers. With the layer thickness of 40 μm used in these experiments, this corresponds to a material thickness of 800 μm of solid material. In the further course of the layers, the emission peak values of almost all specimens approach those of the reference body. Only the test specimen with the lowest surface transition ratio of TR = 16 % shows a constant, albeit relatively small (less than 50 counts), increase in the emission peak value.
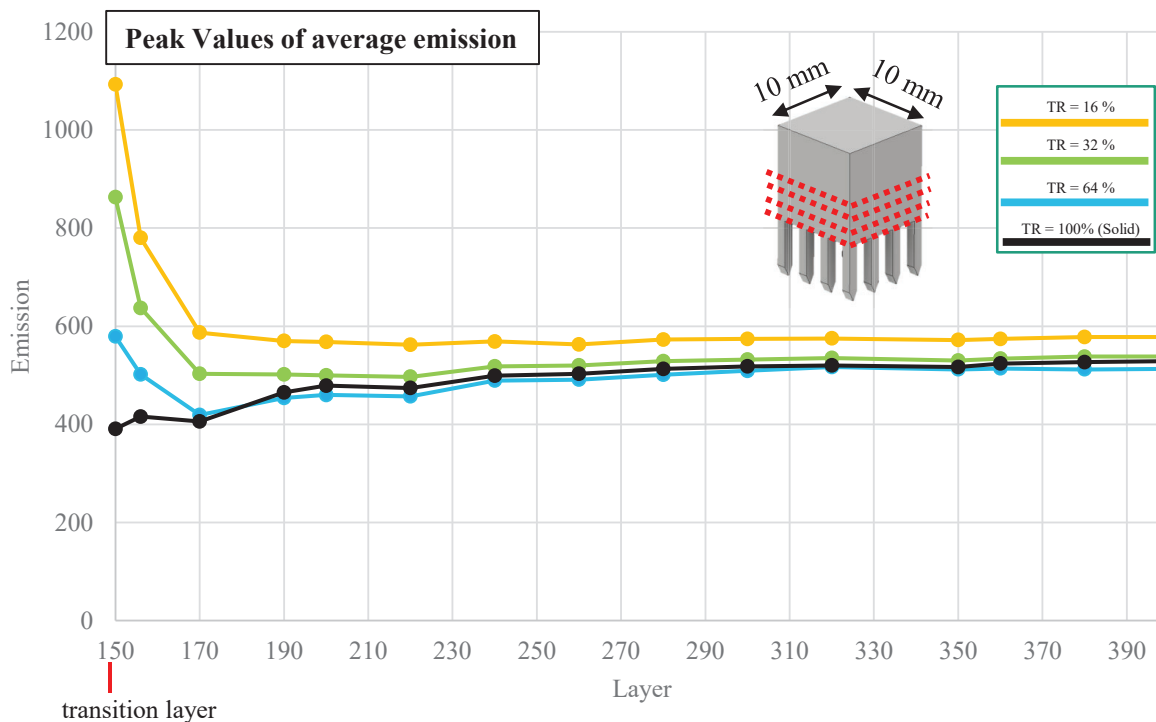

Figure 11: Peak values of average emission in layers for different transition ratios

In the experiment in Figure 10, a relatively strong overheating within the first 20 layers after the surface transition became particularly apparent. In this area, an adaptation of the LPBF process parameters to reduce this overheating could be beneficial with regard to geometry-adapted process control. Figure 12 therefore shows the average emission values for the transition layer for the cube on beams with an area transition ratio of TR = 16 % and a variation of the laser power.
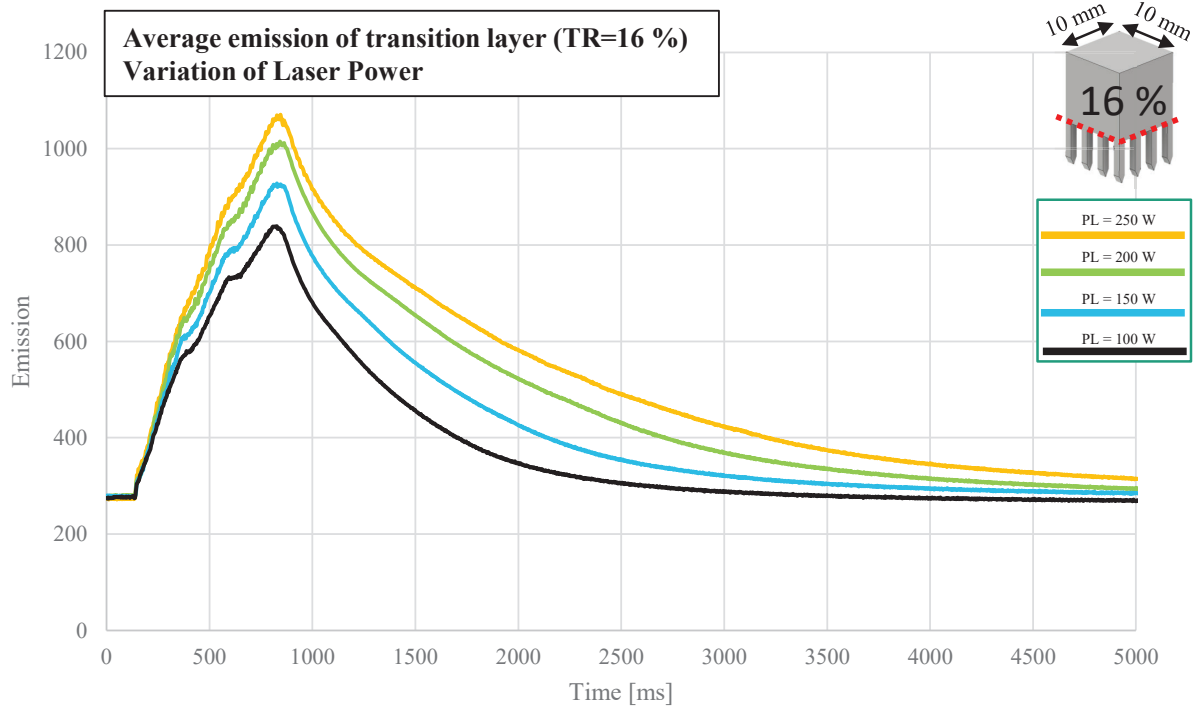

Figure 12: Average emission of transition layer with variation of laser power for TR = 16 %

By reducing the laser power, a reduction of the average emission peak value can be achieved. The maximum emission value of initially approx. 1080 (laser power: 250 W) can be reduced to approx. 810 (laser power: 100 W). Nevertheless, the average peak emission value remains about twice as high as that of the solid reference body (approx. 400) in the previous experiments.
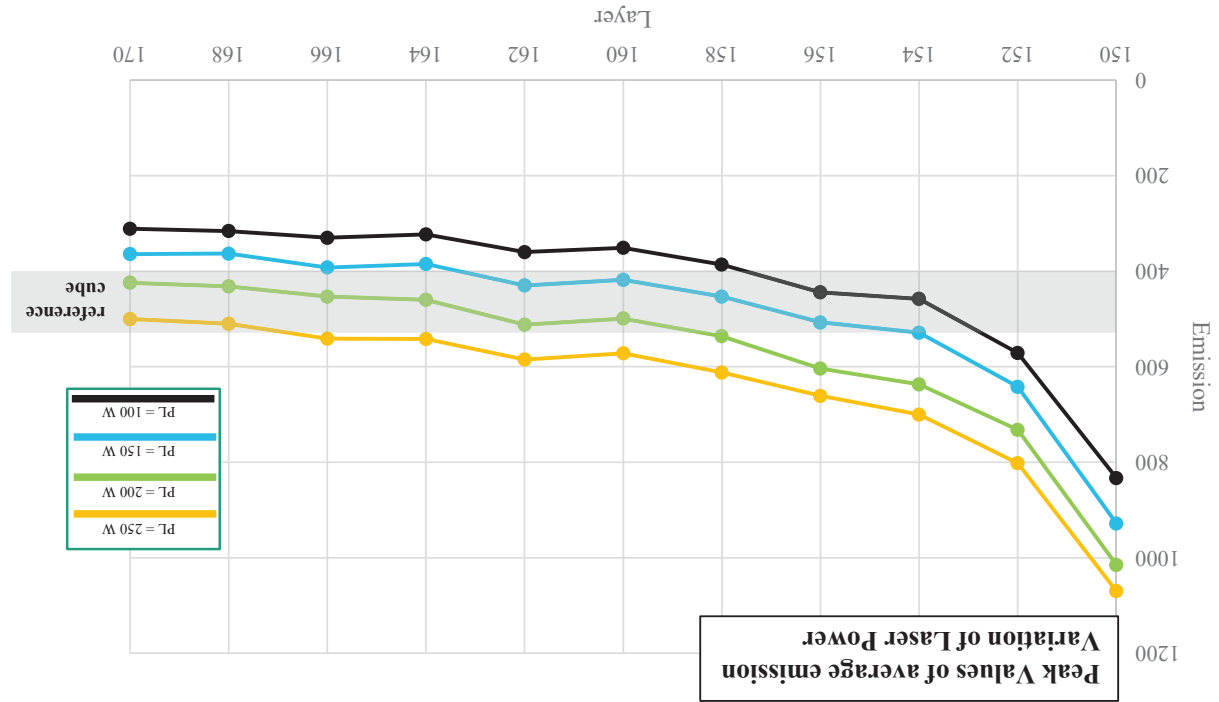
Figure 13 shows the course of the peak values of the average emission for the specimen with TR = 16 %, varying the laser power for the first 20 layers after the transition layer.

Figure 13: Peak values of average emission in layers with variation of laser power for TR = 16 %

After approx. 3 layers, the peak emission value at a power of 100 W is in the emission range of the solid reference body. With increasing layer count, the standard range is undercut, which in practice could involve the risk of porosity within the solidified component material. After 20 layers (layer 170), almost all characteristic curves with reduced power undercut the reference range of the emission. At this point a back-regulation to the reference power of 250 W seems to be expedient.

Conclusion

An approach for the implementation of a geometric-specific process control for the LPBF method is presented. The components to be manufactured are to be divided into a 2D area and a 3D area. The 2D area can be represented by a repetition time model, which can be used to model the spacial and temporal energy input. The 3D area can be characterized by a voxel model to take into account the different geometric properties of the component and to adjust the LPBF process parameters according to the voxel properties.

On an experimental level, exemplary experiments in the 2D range are carried out by constructing web structures of different widths. In the 3D area, cubes are produced on beams to investigate the overheating effects in filigree component areas.

Future work will aim at the determination of the critical repetition time in the 2D range as well as the identification of the relevant voxel properties for the implementation of geometric-

specific process control in the 3D range. Finally a geometric specific parameter map for the material Ti6Al4V shall be derived and demonstrated by the production of complex demonstrator components.

Literature

[1]   Meiners, W. : Direktes selektives Laser-Sintern einkomponentiger metallischer Werkstoffe, Dissertation, RWTH Aachen, 1999.

[2]   Schleifenbaum, H.; Meiners, W.; Wissenbach, K.; Hinke, C.: High Power Selective Laser Melting: A new Approach for Individualizied Series Production, in: 28th International Congress on Applications of Lasers & Electro-Optics, Orlando (ICALEO 2009), FL, 2009.

[3]   Schniedenharn, M. , Schleifenbaum, J. : On the Correlation of the Shielding Gas Flow in L-PBF Machines with Part Density, in DDMC 2018 : Fraunhofer Direct Digital Manufacturing Conference : proceedings : Direct Digital Manufacturing Conference, Berlin, March 14-15, 2018 / Fraunhofer Generativ, Seiten/Artikel-Nr: 289-295

[4]   EOS GmbH Electro Optical Systems, EOS Print 2.0
https://www.eos.info/systeme_loesungen/software/eosprint,
Retrieved: 1.2.2019

[5]   Autodesk Knowledge Network, Advanced Toolpath Utility
https://knowledge.autodesk.com/support/netfabb/
Retrieved: 13.02.2019

[6]   Krauss, H., Qualitätssicherung beim Laserstrahlschmelzen durch schichtweise thermografische In-Process-Überwachung, Dissertation, TU München, 2017

[7]   Cheng, B., Lydon, J., Cooper, K., Cole, V., Northoph, P., Chou, K. Melt Pool Dimension Measurement In Selective Laser Melting Using Thermal Imaging, Solid Freeform Fabrication 2017: Proceedings of the 28th Annual International